ISPRS Journal of Photogrammetry and Remote Sensing 74 (2012) 11–19

Contents lists available at SciVerse ScienceDirect

ISPRS Journal of Photogrammetry and Remote Sensing

journal homepage: www.elsevier.com/locate/isprsjprs

Estimation of vertical plant area density profiles in a rice canopy at different growth stages by high-resolution portable scanning lidar with a lightweight mirror

Fumiki Hosoi, Kenji Omasa *

Graduate School of Agricultural and Life Sciences, The University of Tokyo, Yayoi 1-1-1, Bunkyo-ku, Tokyo 113-8657, Japan

ARTICLE INFO

Article history:
Received 30 March 2012
Received in revised form 11 July 2012
Accepted 20 August 2012
Available online 19 September 2012

Keywords:
Laser beam coverage index
Plant area density
Portable scanning lidar
Rice
Three-dimensional imaging
Voxel-based canopy profiling

ABSTRACT

We used a high-resolution portable scanning lidar together with a lightweight mirror and a voxel-based canopy profiling method to estimate the vertical plant area density (PAD) profile of a rice (*Oryza sativa* L. cv. Koshihikari) canopy at different growth stages. To improve the laser's penetration of the dense canopy, we used a mirror to change the direction of the laser beam from horizontal to vertical (0°) and off-vertical (30°). The estimates of PAD and plant area index (PAI) were more accurate at 30° than at 0°. The root-mean-square errors of PAD at each growth stage ranged from 1.04 to 3.33 $m^2 m^{-3}$ at 0° and from 0.42 to 2.36 $m^2 m^{-3}$ at 30°, and those across all growth stages averaged 1.79 $m^2 m^{-3}$ at 0° and 1.52 $m^2 m^{-3}$ at 30°. The absolute percent errors of PAI at each growth stage ranged from 1.8% to 66.1% at 0° and from 4.3% to 23.2% at 30°, and those across all growth stages averaged 30.4% at 0° and 14.8% at 30°. The degree of laser beam coverage of the canopy (expressed as index Ω) explained these errors. From the estimates of PAD at 30°, regressions between the areas of stems, leaves, and ears per unit ground area and actual dry weights gave standard errors of 7.9 g m^{-2} for ears and 12.2 g m^{-2} for stems and leaves.

1. Introduction

The plant canopy sustains important roles in cycling materials and energy through photosynthesis and transpiration, maintaining plant microclimates, and providing habitats for various species (Monteith, 1973; Jones, 1992; Graetz, 1990; Larcher, 2001). The vertical structure of crop canopies has been studied to explain characteristics such as light distribution within the canopy, light-use efficiency, yield, growth rate, and nitrogen allocation (Imai et al., 1994; Milroy et al., 2001; Takahashi and Nakaseko, 1993; Yunusa et al., 1993). It is often represented by the vertical profile of leaf area density (LAD), which is defined as the one-sided leaf area per unit of horizontal layer volume (Weiss et al., 2004). The leaf area index (LAI) is obtained as the vertical integration of the LAD values. Plant area density (PAD) and plant area index (PAI), which encompass all aboveground organs, are used instead of LAD and LAI when aboveground organs are difficult to separate.

In measuring the structure of crops, it is important to account for changes in the vertical structure with canopy growth. Stratified clipping has been used to obtain LAD and PAD (Imai et al., 1994; Milroy et al., 2001; Monsi and Saeki, 1953; Takahashi and Nakaseko, 1993). This direct method can provide accurate results, but its laborious and destructive nature does not permit repeated measurements of the intact crop structure with canopy growth. The indirect gap-fraction method is widely used for crop measurement with commercially available tools such as cameras with fish-eye lenses and optical sensors (e.g. the Li-Cor LAI-2000 plant canopy analyzer; Bréda, 2003; Grantz et al., 1993; Hanan and Bégué, 1995; Welles and Cohen, 1996). Although it allows automatic data collection and nondestructive measurement of canopy structure, the accuracy of measurement is affected by the spatial distribution of leaves and by sunlight conditions (Chason et al., 1991; Weiss et al., 2004).

In the last decade, lidar (light detection and ranging) has been emerged as a powerful tool for three-dimensional measurements of various purposes, e.g. city modeling (Pu and Vosselman, 2009), topography mapping (Webster et al., 2006), cultural heritage surveys (Pesci et al., 2012). This technology has been also utilized for structural measurements of plant canopies (Brandtberg et al., 2003; Harding et al., 2001; Holmgren and Persson, 2004; Hosoi et al., 2005, 2010, 2011; Hosoi and Omasa, 2006, 2007, 2009a,b; Hyyppä et al., 2001; Lefsky et al., 2002; Næsset et al., 2004; Omasa et al., 2000, 2002, 2003, 2007a,b; Riaño et al., 2003). Lidar can provide 3D information by calculating the distance between the sensor and the target from the elapsed time between the emission

* Corresponding author. Tel.: +81 3 5841 5340; fax: +81 3 5841 8175.
E-mail address: aomasa@mail.ecc.u-tokyo.ac.jp (K. Omasa).

0924-2716/$ - see front matter © 2012 International Society for Photogrammetry and Remote Sensing, Inc. (ISPRS) Published by Elsevier B.V. All rights reserved.
http://dx.doi.org/10.1016/j.isprsjprs.2012.08.001

and return of laser pulses (the time-of-flight method) or from the difference in the phases of the modulation between them (phase-shift method) or by trigonometry (optical-probe or light-section methods). Airborne lidars with a large footprint (typically 10–25 m in diameter) and a large scan width have been developed for a target of forest remote sensing on large scales (Harding et al., 2001; Lefsky et al., 2002). These systems include a waveform-recording device that digitizes the power level of the entire return laser signal from canopy elements and the ground. Although they are sufficient for large scale measurement, the image resolution has been insufficient to provide detailed descriptions of canopy structure at the level of individual plants. Meanwhile, current airborne small-footprint lidar (the footprint diameter is typically 10–30 cm) has made it possible to measure canopy structures with fine spatial resolution (Brandtberg et al., 2003; Holmgren and Persson, 2004; Hyyppä et al., 2001; Næsset et al., 2004; Omasa et al., 2000, 2003; Riaño et al., 2003). The lidar system functions as a discrete-return recording device, since it only receives a single return signal or a small number of return signals from the canopy and ground. At the use of this system, there was a tendency for tree height to be underestimated when the laser pulse density was insufficient to detect the actual tree tops (<1 pulse per m^2). Recent advances in lidar technology have increased the pulse density to >10 pulse per m^2, with a pulse repetition frequency of >200 kHz, so that the probability of laser hits on the actual tops of the trees increases and the magnitude of the underestimation is reduced (Omasa et al., 2003). This type of lidar has been used for estimating the LAI values of tree species (Magnussen and Boudewyn, 1998; Morsdorf et al., 2006) and also of crops (Houldcroft et al., 2005). However, these studies mainly focused on LAI estimation rather than on the estimation of the vertical LAD or PAD profiles, because they captured insufficient information about the vertical canopy structure to estimate the latter.

Although portable ground-based nonscanning lidar has been used in several studies of vertical foliage profiles (Parker et al., 2004; Radtke and Bolstad, 2001), portable ground-based scanning lidar is now more popular for the measurement (Henning and Radtke, 2006; Hosoi and Omasa, 2006, 2007, 2009a,b; Lovell et al., 2003; Omasa et al., 2002, 2007a,b; Takeda et al., 2005; Tanaka et al., 2004; Urano and Omasa, 2003; van der Zande et al., 2006). The latter can record much 3D data quickly and nondestructively. The efficient data collection and portability of this technology are advantageous for repeated measurements of crops over time. Commonly used portable ground-based scanning lidar systems are discrete-return recording systems at which a single or a small number of return signals from the canopy are received. In addition to the system, the waveform-recording ground-based scanning lidar system has been also utilized for canopy structural measurement (Strahler et al., 2008), by which more structural information can be extracted from the internal canopy. Thus, those technologies promise to overcome the shortcomings of the conventional means of measuring the vertical structure of crops.

Recently, we demonstrated that the vertical PAD profiles of a wheat canopy at different growth stages can be measured accurately by high-resolution portable scanning lidar with a resolution of about 1 mm at a range of about 5 m through a voxel-based canopy profiling (VCP) method (Hosoi and Omasa, 2009a). Besides a wheat canopy, it is significant for the method to be applied to other crops. Rice is one of the main crops in the world and so it is important to understand the characteristics. If the VCP method is applicable to rice canopies, the resultant vertical canopy profiles would give useful information for well understanding of the characteristics. However, a rice canopy is denser than a wheat canopy, so laser penetration might be restricted. We found that a more vertical laser beam penetrates a dense rice canopy better than a horizontal beam (Hosoi and Omasa, 2012). However, this is difficult to achieve in the field, because the lidar needs to be held above the target.

We estimated the vertical profiles of a rice canopy at different growth stages using a high-resolution portable scanning lidar and a mirror oriented at different angles to achieve vertical penetration, and compared the results with direct measurements. To assess the accuracy of the PAD estimates, we investigated the relationships between an index of laser beam coverage and the errors in PAD estimates. We propose a way to estimate the dry weight of each plant organ from the resultant PAD values.

2. Materials and methods

2.1. Plant material

The experiment was conducted in 2010 in a paddy field in Ibaraki Prefecture, 40 km northeast of central Tokyo, Japan (35°56′N, 140°04′E). Rice (*Oryza sativa* L. cv. Koshihikari) seedlings were transplanted on 1 May with 30-cm inter- and intra-row spacings. Four square plots (1.2 m × 1.2 m) were established for measurements of four growth stages, on 27 May (early tillering), 17 June (late tillering), 13 July (panicle formation), and 14 August (maturity).

2.2. Lidar measurements

We used a high-resolution portable scanning lidar that calculates distances by trigonometry (a modified TDS-130L 3-D laser scanner; Pulstec Industrial Co., Ltd., Japan) to make 3D measurements of the rice canopy. The size is 640 × 263 × 175 mm and the weight is 12.0 kg. The measurable range is 3.5–10 m. The range and scan resolutions are about 1 and 2 mm, respectively, at a range of about 5 m. A rotating mount with a stepper motor and a galvano-mirror within the lidar head automate the horizontal and vertical scanning. The range of scanning angle is ±45° for horizontal and ±20° for vertical. The wavelength of the laser beam is 786 nm and the beam diameter is 5 mm at 3.5 m. The maximum laser beam output power is 30 mW (equivalent to class 3B laser product according to IEC60825-1). The data sampling rate is 1.25 ms per point.

The lidar was installed on a bund near the measurement plots (Fig. 1A). A thin-film mirror measuring 1.0 m × 1.5 m (Refex; J. Front Design & Construction Co., Ltd., Japan) was mounted above the crop (1.5 m above the ground) on rails to reflect the laser's beam down onto the canopy. Since the mirror is made of an evaporation–deposition aluminum–plastic film, at 3.8 kg it is much lighter than a glass mirror and thus it was easy to handle in the field. The mirror's reflectance is about 90% at the laser wavelength of 786 nm. Since the laser beams are reflected twice on the mirror until they return to the lidar sensor, the returning laser beam power decreases to about 80% of the power at the normal (no mirror) setting. This might cause the decrease of the number of returning laser beams detected at the lidar sensor. Then the emitted laser beam power was adjusted to the maximum (30 mW) to keep the returning beam power enough to be detected at the lidar sensor, so that the number of detected returning beams did not decrease by using the mirror.

The rails were arranged on the field horizontally along a laser beam direction of the lidar scan. The mirror could be slid along the rails at 3.3–6.9 m from the lidar, that was equivalent to 4.8–8.4 m of the beam path length from the lidar to the ground under the target canopy with reflection on the mirror when the beam direction into the canopy is vertical (see Fig. 1C). It could also pivot on its base so that the laser beam could be directed into the canopy at different angles (defined as the central zenith angle, θ_c; Fig. 1B

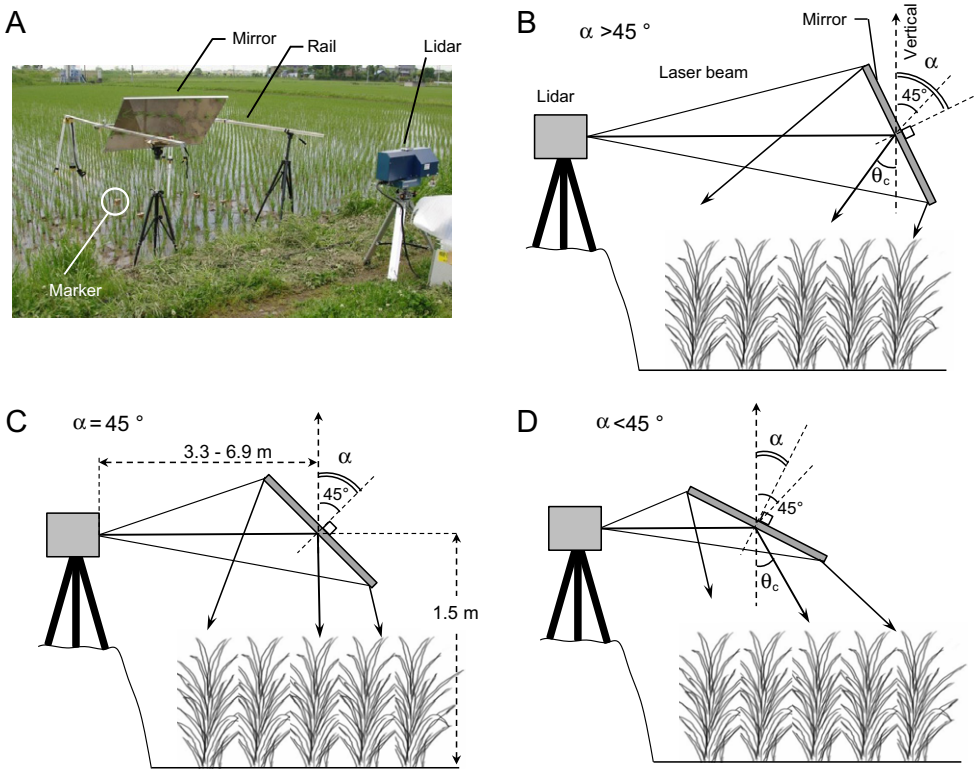

Fig. 1. Measurement of the rice canopy by high-resolution portable scanning lidar and adjustable mirror. (A) Field set-up. (B–D) Relation of beam direction and mirror angle. α: Zenith angle of the normal to the mirror surface. θ_c: Central zenith angle of laser beam.

and D). Measurements were taken at θ_c = 0° and 30° on each occasion. To achieve a θ_c of 0° (vertical illumination), the zenith angle of the normal to the mirror surface, α, was set at 45° (Fig. 1C). To achieve a θ_c of 30° (off-vertical illumination), α was set both at >45° (Fig. 1B) and at <45° (Fig. 1D), where laser beams were towards the lidar position and towards the opposite side of the lidar position, respectively. Since laser beams could illuminate the different sides of the canopy by these settings, more laser beam penetration into the interior was expected. The mirror was not big enough to cover the plot, so it was moved along the rails to cover it in two scans in each of the settings. Thus, the total numbers of the scans were two for θ_c of 0° and four for θ_c of 30°. Through those measurements, six cubic markers that were attached to poles and placed around the plot (see Fig. 1A) were also scanned together with the target canopy. The markers within the lidar data were used as reference points for registration of each set of the lidar data.

2.3. Direct measurements

To validate the lidar-derived estimates, we directly measured LAD and PAD in horizontal layers by stratified clipping within each plot. On each date, all plants within each plot were clipped in layers 5 cm thick (27 May) or 10 cm thick (17 June–14 August), and the clippings were separated into leaves, stems, and ears. The areas of each were measured with a commercially available desktop scanner (ScanBit MFS-A3; Exemode, Inc., Japan; details in Hosoi and Omasa, 2009a). The PAD of each organ in each layer was calculated as the projected area of each organ (see Section 2.4) per unit of horizontal layer volume (0.07 m^3 for 27 May and 0.14 m^3 for 17 June–14 August). The PAI was obtained as the vertical integration of the PAD of all organs. The LAI was obtained as the vertical integration of the LAD. After the PAD measurement, all of the organs were dried in an oven at 80 °C for 3 days and weighed.

2.4. Computation of plant area density

PAD was computed by the VCP method (Hosoi and Omasa, 2006). The complete point-cloud data set for each of the laser beam incidence angles was registered into a single point-cloud data set with a common 3D coordinate system for each measurement date using the iterative closest-point algorithm (Besl and McKay, 1992) with the reference points of six cubic markers (described in Section 2.2). All points in the registered data set were converted into voxel coordinates. The voxel size was set to 1 mm in recognition of the lidar's resolution (1–2 mm). Voxels converted from points within the data set were given an attribute value of 1. All laser beams emitted from each lidar position were traced within the voxel array in accordance with the actual beam angles and the mirror angles. Voxels through which one or more beams passed without touching the canopy were given an attribute value of 2. From the attribute values, PAD in each horizontal layer was computed as (Hosoi and Omasa, 2006):

$$\mathrm{PAD} = \frac{\cos\theta_c}{G(\theta_c)} \cdot \frac{1}{\Delta H} \sum_{k=m_h}^{m_{h+\Delta H}} \frac{n_l(k)}{n_l(k) + n_p(k)}. \quad (1)$$

where θ_c is the central zenith angle of a laser beam; $n_l(k)$ and $n_P(k)$ are the numbers of voxels with attributes of 1 ("intercepted") and 2 ("passed through"), respectively, in the kth horizontal layer of the voxel array (thus, $n_l(k) + n_P(k)$ represents the total number of incident beams that reach the kth layer); ΔH is the horizontal layer thickness (=0.05 m for 27 May and 0.10 m for 17 June–14 August); and m_h and $m_{h+\Delta H}$ are the voxel coordinates on the vertical axis equivalent to heights h and $h + \Delta H$ in orthogonal coordinates ($h = m_h \times \Delta k$). $G(\theta_c)$ is the mean projection of a unit leaf area on a plane perpendicular to the direction of the laser beam at θ_c (Norman and Campbell, 1989; Weiss et al., 2004; Welles and Norman, 1991). The term $\cos\theta_c\,[G(\theta_c)]^{-1}$ corrects for the influence of leaf inclination angle and laser beam direction; the distribution of leaf inclination

angles is required to determine its value. Each leaf was distinguishable in the lidar images of each growth stage because of the fine resolution. After each leaf was extracted from the images, it was divided lengthwise into 15-mm segments, and 200 segments were randomly selected. Points within each of the pieces were fitted by a plane based on a least square method and normals to the planes were estimated. The distribution of leaf inclination angles at each growth stage was derived from the angles of these normals with respect to the zenith. From the PAD estimates computed for each horizontal layer, the vertical PAD profiles at $\theta_c = 0°$ and 30° on each measurement date were obtained and compared with the directly measured profiles. In addition, PAI values at each growth stage were estimated as the vertical integration of the PAD estimates and the accuracy was examined.

2.5. Derivation of the laser beam coverage index

A laser beam coverage index, Ω, can be used to predict the error of LAD estimates obtained by different types of lidar and with different beam settings (Hosoi et al., 2010):

$$\Omega = A_{\text{beam}} \times N_0 \exp(-K \cdot LAI_{\text{cum}}) \quad (2)$$

where A_{beam} is the horizontally projected area of the laser beam; N_0 is the initial number of incident laser beams just before entry into the canopy per unit area of a horizontal plane; K accounts for the influence of the leaf inclination angle and the angle of incidence of laser beams (the inverse of the correction factor $\cos\theta_c\ [G(\theta_c)]^{-1}$ in Eq. (1)); and LAI_{cum} is the lidar-derived cumulative LAI at a certain height (equivalent to cumulative PAI in this study). Ω indicates the proportion of the area of a horizontal plane within the canopy covered by laser beams. The index is adapted here to PAD estimates as:

$$\Omega = A_{beam} \times N \quad (3)$$

where N is equivalent to the term $N_0\exp(-K{\cdot}LAI_{cum})$ in Eq. (2) but means the number of incident laser beams per unit area of a horizontal plane at a given height. Since N could be derived directly together with PAD by the VCP method in Section 2.4, Ω was calculated by Eq. (3) rather than by Eq. (2). Then we investigated the relationships between Ω and the absolute errors of the corresponding PAD estimates at $\theta_c = 0°$ and 30°.

2.6. Correlation between lidar-derived areas of aboveground organs and dry weights

The errors of the lidar-derived PAD profiles at $\theta_c = 0°$ and 30° showed which angle gave more accurate results. The more accurate values were used in the following calculations. The lidar-derived total areas of stems and leaves per unit ground area at each growth stage were obtained by multiplying the lidar-derived PAD by the layer thickness and summing up the values vertically. The area corresponding to ears was subtracted from the total as described below to give the total areas of stems and leaves on 14 August. We investigated the correlation of the total areas with the corresponding actual stem and leaf dry weights.

The PAD estimates corresponding to ears on 14 August were separated by multiplying the lidar-derived PAD above 50 cm by the ratio of ear to total surface area obtained from direct measurements of each layer. The PAD was converted into area of ears per unit ground area in each layer by multiplication with the layer thickness (=0.1 m). We investigated the correlation of the area of ears with the corresponding actual ear dry weights.

3. Results

The directly measured PAD values were larger in lower layers on 27 May (Fig. 2A). The distribution spread to higher layers as

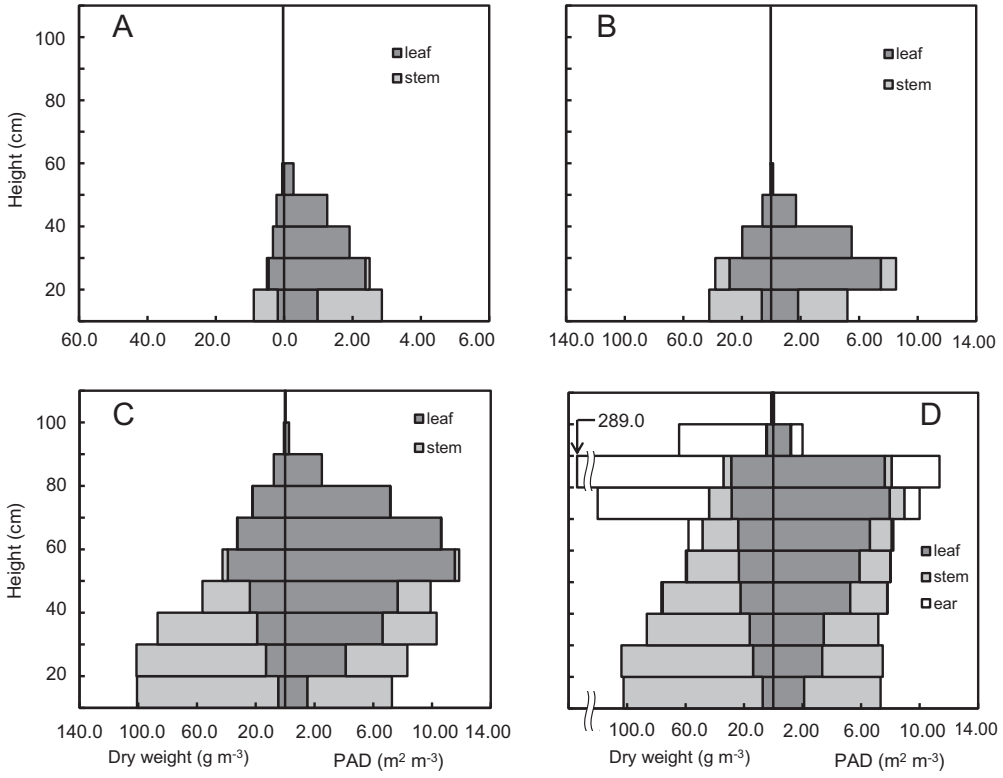

Fig. 2. Directly measured vertical PAD and dry weight distributions of leaf, stem, and ear within a rice canopy obtained by stratified clipping. (A) 27 May, tillering; (B) 17 June, tillering; (C) 13 July, panicle forming; (D) 14 August, maturing.

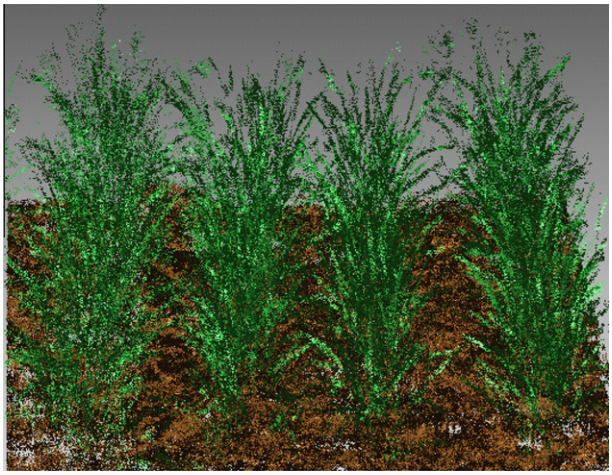

Fig. 3. Image of the rice canopy on 17 June obtained by co-registration of images measured by lidar at $\theta_c = 30°$. Shading effect is added to this image by changing brightness of each point.

the crop grew, along with the peaks in the distribution (Fig. 2B–D). Leaves dominated in the middle to higher layers and stems in the lower layers. Ears became dominant in the upper layers on 14 August. The PAI values were 0.44 (27 May), 2.10 (17 June), 6.82 (13 July), and 6.94 $m^2\ m^{-2}$ (14 August), and the LAI values were 0.34, 1.67, 5.20, and 4.35 $m^2\ m^{-2}$, respectively. The dry weight in each layer increased with canopy growth (Fig. 2). Stems contributed greatly to the dry weight in lower layers on 27 May and 17 June and in lower to middle layers on 13 July and 14 August. Ears contributed greatly to the dry weight in the upper layers on 14 August. The total dry weights were 20.1 (27 May), 106.8 (17 June), 451.2 (13 July), and 962.8 g m^{-2} (14 August). The total ear dry weight on 14 August was 403.1 g m^{-2}.

In a co-registered image of the rice canopy on 17 June at $\theta_c = 30°$, where shading effect is added to this image by changing brightness of each point, each leaf is clearly distinguishable because of the fine resolution of the image (Fig. 3).

The lidar-derived distributions of the leaf inclination angle of the canopy showed a peak at 65° on 27 May, with the distribution tailed to lower angles (Fig. 4A). The distribution was approximately the same on 17 June with a weak peak around 55° (Fig. 4B). Although the distribution shifted to higher angles with a peak at 80° on 13 July (Fig. 4C), it moved to lower angles with a peak at 15° on 14 August (Fig. 4D).

At $\theta_c = 30°$, although the actual PAD profiles changed greatly as the canopy grew, the lidar-derived PAD estimates were good except in the lowest layers on 27 May (greatly underestimated) and 14 August (greatly overestimated) (Fig. 5). On 13 July and 14 August, the lidar-derived PAD was slightly overestimated in the layers corresponding to the peak and below. At $\theta_c = 0°$, the lidar-derived values underestimated PAD at all growth stages in most layers (except, for example, at 40 cm on 14 August, with an overestimate). In particular, the underestimation was large on 27 May and 17 June, and in the layer corresponding to the peak of actual PAD on 13 July. At $\theta_c = 30°$, the root-mean-square errors (RMSEs) of the PAD estimates were 0.69 (27 May), 0.42 (17 June), 0.99 (13 July), and 2.36 $m^2\ m^{-3}$ (14 August). At $\theta_c = 0°$, the RMSEs were 1.04, 3.33, 1.32, and 1.33 $m^2\ m^{-3}$, respectively. At $\theta_c = 30°$, the absolute percent errors of the PAI estimates were 22.9%, 4.8%, 4.3%, and 23.2%, respectively. At $\theta_c = 0°$, they were 42.9%, 66.1%, 10.9%, and 1.8%, respectively.

Across all growth stages, the relationship between directly measured and lidar-derived PAD values was more accurate at $\theta_c = 30°$ (RMSE = 1.52 $m^2\ m^{-3}$, absolute percent error = 13.8%) than at $\theta_c = 0°$ (RMSE = 1.79 $m^2\ m^{-3}$, absolute percent error = 30.4%; Fig. 6). As shown in Fig. 5, there was an overall tendency for overestimation at $\theta_c = 30°$ (Fig. 6A) and underestimation at $\theta_c = 0°$ (Fig. 6B).

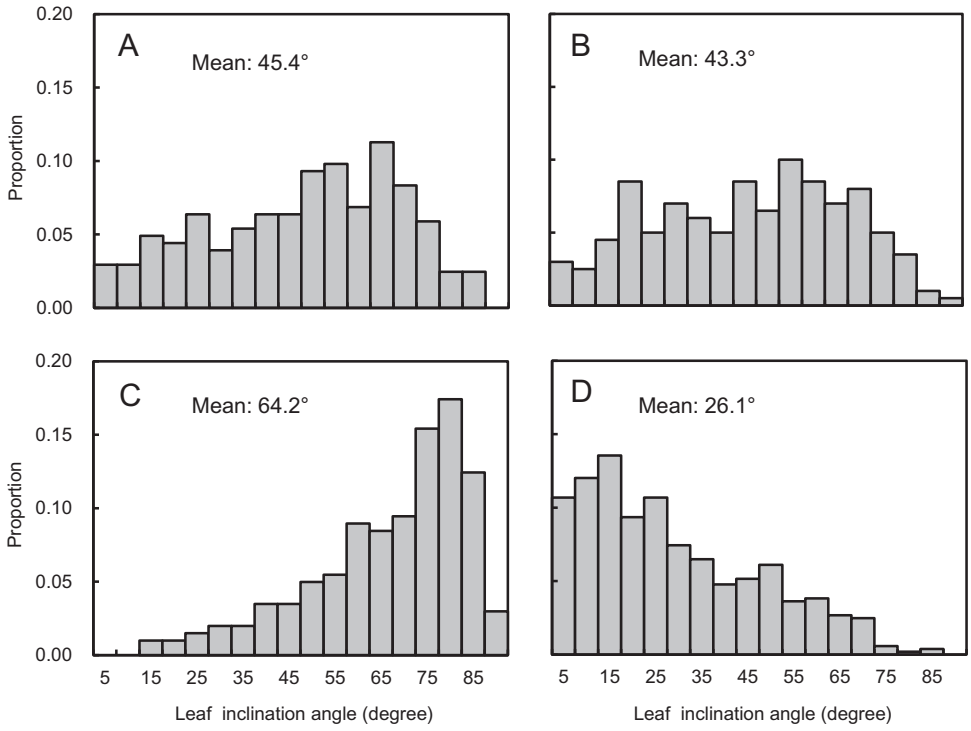

Fig. 4. Distributions of leaf inclination angles in rice canopy derived from lidar images. (A) 27 May, tillering; (B) 17 June, tillering; (C) 13 July, panicle forming; (D) 14 August, maturing. "Mean" indicates mean leaf inclination angle.

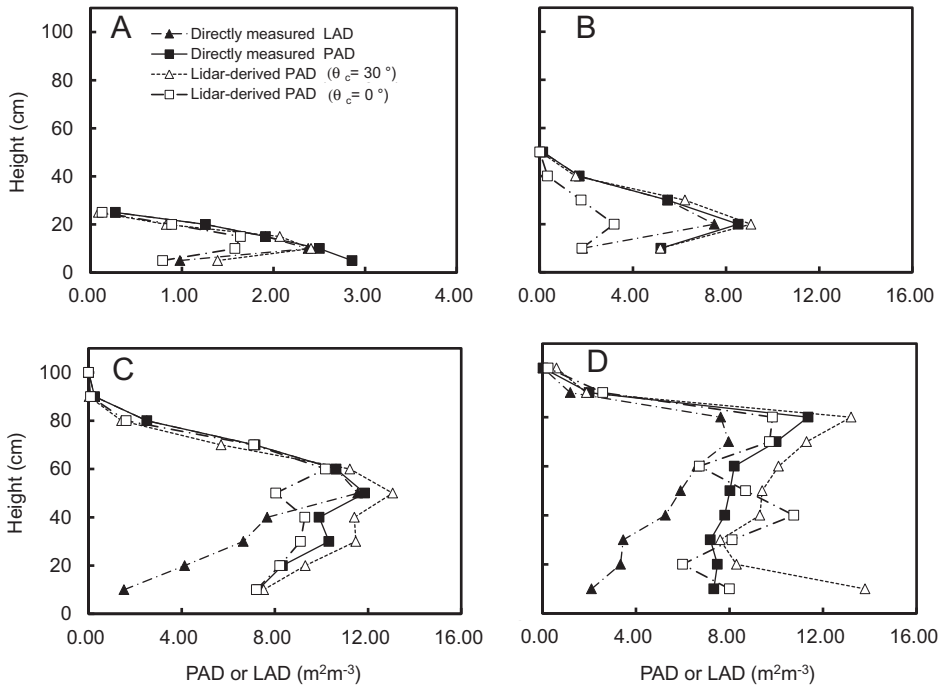

Fig. 5. Comparison of profiles among lidar-derived PAD at $\theta_c = 0°$ and 30°, directly measured PAD (modified from Hosoi and Omasa, 2012), and directly measured LAD at each growth stage. (A) 27 May, tillering; (B) 17 June, tillering; (C) 13 July, panicle forming; (D) 14 August, maturing.

When the index of laser beam coverage, Ω, decreased to around 2, the absolute errors of the PAD estimates at both angles began to increase (Fig. 7). Large errors were associated with $\Omega \leqslant \sim 1.0$, at which the errors were larger at $\theta_c = 0°$ than at $\theta_c = 30°$. Smaller errors were associated with values of $\Omega > 2.0$.

Lidar-derived areas of stems and leaves were linearly correlated with actual dry weights, with $R^2 = 0.99$ and a standard error of 12.2 g m^{-2} (Fig. 8A). Ears also showed a linear correlation, with $R^2 = 0.94$ and the standard error of 7.9 g m^{-2} (Fig. 8B).

4. Discussion

The angle of incidence of laser beams into a canopy affects the number of beams that penetrate the interior and thus relates to the accuracy of LAD or PAD estimation (Hosoi and Omasa, 2007). To improve the accuracy of estimation, the angle should depend on the canopy structure. However, it can be difficult to set the angle freely in the field, because this requires the position of the lidar to be moved. In particular, setting a near-vertical angle of laser incidence is often difficult because a heavy weight lidar instrument must be placed at a higher place above or around the canopy. In the case of the present study, the lidar whose weight is 12.0 kg must be placed at least 4.8 m height (equivalent to minimal beam path length in the vertical beam incidence into the canopy, described in Section 2.2) above the canopy if the mirror was not used. Use of light weight lidar instruments (e.g. Rosell et al., 2009; van der Zande et al., 2006) may ease such setting, but the performance of such systems (e.g. measurable range, scanning performance, range accuracy, etc.) is not still insufficient to use the accurate measurement of vertical canopy structure. Thus, in the case of a low target such as rice, the angle of incidence is restricted to near-horizontal due to the difficulty of a way to place the lidar above the canopy or a higher place around the canopy. Our method removes such a limitation through the use of an adjustable lightweight mirror that can be easily handled and installed in the field.

In a previous study (Hosoi and Omasa, 2009a), we used an incidence angle of 57.5° in a wheat canopy, because it allowed for the correction factor ($\cos(\theta_c)\,[G(\theta_c)]^{-1}$; see Eq. (1)) to be approximated as a constant value. Since this angle is more horizontal than vertical, the path of the laser beam within the canopy is longer than the path at a more vertical angle. A longer path length decreases the likelihood that a laser beam will reach the middle and lower part

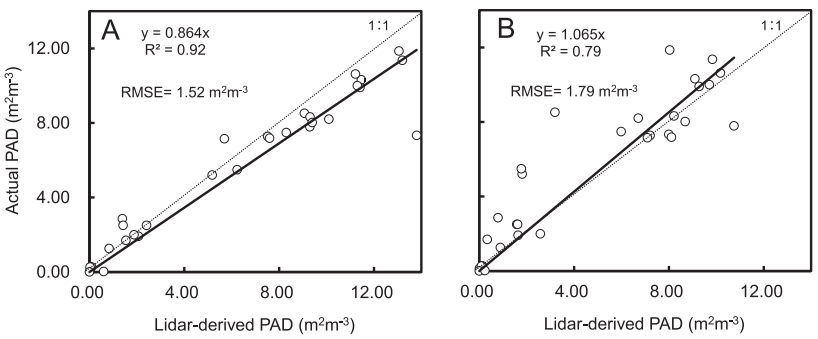

Fig. 6. Relationship between directly measured and lidar-derived PAD at all growth stages. (A) $\theta_c = 30°$; (B)=0°. RMSE: root-mean-square error.

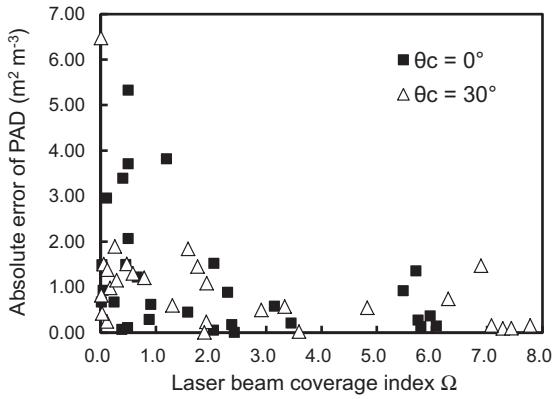

Fig. 7. Relationships between the laser beam coverage index (Ω) and the absolute errors of PAD at $\theta_c = 0°$ and 30°.

of the canopy. This is not a problem for the lower PAD values of a wheat canopy, but is likely to be a problem for the higher PAD values of a rice canopy (at maturity, the mean directly measured PAD value of the rice canopy was 2.1 times that of the wheat canopy in Hosoi and Omasa, 2009a). The mirror allowed the path length in the rice canopy to be shortened by selecting more vertical angles.

At both values of θ_c, Ω was related to the PAD errors in each layer at all growth stages. Theoretically, when $\Omega > 1.0$, the laser beams can illuminate the entire horizontal plane, so the PAD error decreases. When $\Omega < 1.0$, some parts of the horizontal plane cannot be illuminated, so the error increases owing to a lack of information about the canopy. In practice, Ω should be >2.0 (Fig. 7). The results in Fig. 7 show that laser beam coverage within the canopy can well explain the errors of estimation of the PAD of a rice canopy, and the value can be used to judge the accuracy of the PAD estimates. As shown in Eq. (2), the index Ω is composed of the laser beam settings A_{beam} and N_0, and the canopy structural attributes K and LAI_{cum} (LAI_{cum} is equivalent to PAI_{cum} in this study). K is expressed by $G(\theta_c)$ $(\cos\theta_c)^{-1}$, which depends on the leaf inclination angle distribution and the angle of incidence of laser beams (equivalent to θ_c). Thus, factors affecting the accuracy of estimation of the PAD of a rice canopy are PAI_{cum}, A_{beam}, N_0, the leaf inclination angle distribution and the angle of incidence of laser beams.

Although our results were collected by a high-resolution portable scanning lidar and relate to rice (a grass), similar results pertaining to LAD estimation have been collected by a moderate-resolution, portable scanning lidar and an airborne scanning lidar in relation to broadleaf trees (Hosoi et al., 2010). This shows the general applicability of Ω for different plant species and different lidar instruments.

Although the PAD estimation errors were large when $\Omega < 2.0$, the errors were larger at $\theta_c = 0°$ than at $\theta_c = 30°$ (Fig. 7). The points with the largest errors correspond to the low PAD estimates at $\theta_c = 0°$ on 27 May and 17 June (Fig. 5A and B). The differences in the PAD estimates on these dates between the two angles affected the overall accuracy at all growth stages, resulting in the overall better estimates at $\theta_c = 30°$ than at $\theta_c = 0°$ (Fig. 6). A possible cause of the difference is the difference in the quantity of obstructed leaves (blocked by other leaves) at each angle (Hosoi and Omasa, 2007). The presence of these leaves causes an error in PAD estimation, even if the same number of laser beams intersect the canopy at each angle. The degree of obstruction can be reflected in $G(\theta_c)$ in Eq. (1) (Hosoi and Omasa, 2007). The degree of obstruction increases as the value of $G(\theta_c)$ increases. In our rice canopy, the mean values of $G(\theta_c)$ were 0.65 at $\theta_c = 0°$ and 0.59 at 30° on 27 May, and 0.67 and 0.60 on 17 June. Thus, the obstruction is a possible cause of the difference in accuracy between the two angles.

Although the PAD values at $\theta_c = 30°$ were well estimated overall, they were greatly overestimated in the lowest layer in August. This overestimation would relate to the distribution of leaf inclination angle, which changed greatly from erectophile to planophile from July to August with lodging. The planophile distribution increased the probability of the laser beams' hitting the leaves at the near-vertical beam angle, reducing the number of beams reaching the lowest layer. In the lowest layer, $\Omega = 4.7 \times 10^{-3}$: this very low value explains the large error.

As in the wheat canopy (Hosoi and Omasa, 2009a), the dry weights of ears, leaves, and stems in the rice canopy could be also estimated from a regression between the dry weight and lidar-derived area of each organ. Lidar-derived dry weight estimates can offer useful information on growing conditions and for agricultural management and carbon budgeting.

In the present study, use of an adjustable lightweight mirror removed a limitation of the allowable laser beam angle of incidence, so that measurements at more vertical angles appropriate for arice canopy could be effectively conducted. Consequently our proposed method with the mirror greatly contributed to obtaining good results of the PAD estimation and useful knowledge about the structural features of a rice canopy and the measurement method. In the future works, by selecting a long range lidar system and considering the setting points of the mirror and the lidar, this method may be useable to mitigate the limitation of the laser beam angle of incidence for other plants with tall canopies.

5. Conclusion

The vertical PAD profile of a rice canopy at different growth stages can be estimated through the use of a high-resolution por-

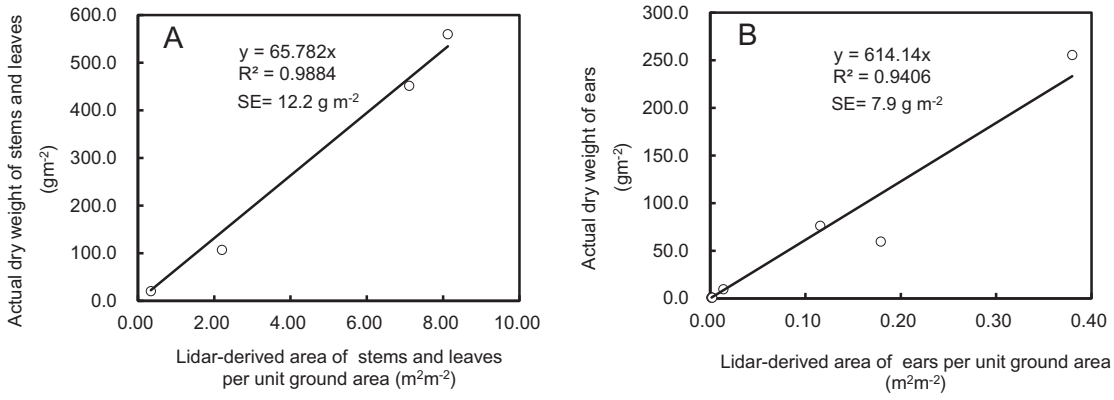

Fig. 8. Relationships between lidar-derived area per unit ground area and actual dry weight. (A) Stems and leaves; (B) ears. SE, standard error.

table scanning lidar together with a lightweight mirror and the VCP method. The angle of incidence of the laser beam into the canopy needed to be nearly vertical to cope with the high PAD values of the canopy. This was achieved with a simple mirror installed above the crop to deflect the laser beam. The PAD profiles at each growth stage were computed by the VCP method from co-registered data. They were well estimated overall at the incidence angle of 30°, with a few exceptions (e.g. the lowest part on 14 August). It was shown that the laser beam coverage within canopy expressed as the index Ω can well explain the errors of PAD estimates and thus the index can be used to judge the accuracy. Since the index is composed of structural attributes of canopy and lidar settings, the attributes and the settings were shown to be factors affecting the accuracy of the PAD estimates in the rice canopy. Ω could be used to estimate the accuracy of estimation in a rice canopy as well as the other plant reported in previous works. These and previous results show the general applicability of Ω to various plant species and lidar instruments. The degree of obstruction of leaves could explain the difference in the PAD errors between the angles of incidence. The lidar-derived PAD could be used to estimate the dry weight of ears, leaves, and stems.

The use of a lightweight mirror released the limitation on the angle of incidence of the laser beam in the field. In spite of the high density of the rice canopy, the PAD of different growth stages could be well estimated by a near-vertical laser beam. To use the method, it is essential to configure the lidar and mirror to maximize Ω and minimize $G(\theta_c)$. Future work should investigate the applicability of our method to other field conditions and species.

References

Besl, P.J., McKay, N.D., 1992. A method for registration of 3-D shapes. IEEE Transactions on Pattern Analysis and Machine Intelligence 14 (2), 239–256.

Brandtberg, T., Warner, T.A., Landenberger, R.E., McGraw, J.B., 2003. Detection and analysis of individual leaf-off tree crowns in small footprint, high sampling density lidar data from the eastern deciduous forest in North America. Remote Sensing of Environment 85 (3), 290–303.

Bréda, N.J.J., 2003. Ground-based measurements of leaf area index: a review of methods, instruments and current controversies. Journal of Experimental Botany 54 (392), 2403–2417.

Chason, J.W., Baldocchi, D.D., Huston, M.A., 1991. A comparison of direct and indirect methods for estimating forest canopy leaf area. Agricultural and Forest Meteorology 57 (1–3), 107–128.

Graetz, R.D., 1990. Remote sensing of terrestrial ecosystem structure: an ecologist's pragmatic view. In: Hobbs, R.J., Mooney, H.A. (Eds.), Remote Sensing of Biosphere Functioning. Springer, New York, pp. 5–30.

Grantz, D.A., Zhang, X.J., Metheney, P.D., Grimes, D.W., 1993. Indirect measurement of leaf area index in Pima cotton (*Gossypium barbadense* L.) using a commercial gap inversion method. Agricultural and Forest Meteorology 67 (1–2), 1–12.

Hanan, N.P., Bégué, A., 1995. A method to estimate instantaneous and daily intercepted photosynthetically active radiation using a hemispherical sensor. Agricultural and Forest Meteorology 74 (3–4), 155–168.

Harding, D.J., Lefsky, M.A., Parker, G.G., Blair, J.B., 2001. Laser altimeter canopy height profiles methods and validation for closed-canopy, broadleaf forests. Remote Sensing of Environment 76 (3), 283–297.

Henning, J.G., Radtke, P.J., 2006. Ground-based laser imaging for assessing three-dimensional forest canopy structure. Photogrammetric Engineering and Remote Sensing 72 (12), 1349–1358.

Holmgren, J., Persson, Å., 2004. Identifying species of individual trees using airborne laser scanner. Remote Sensing of Environment 90 (4), 415–423.

Hosoi, F., Omasa, K., 2006. Voxel-based 3-D modeling of individual trees for estimating leaf area density using high-resolution portable scanning lidar. IEEE Transactions on Geoscience and Remote Sensing 44 (12), 3610–3618.

Hosoi, F., Omasa, K., 2007. Factors contributing to accuracy in the estimation of the woody canopy leaf-area-density profile using 3D portable lidar imaging. Journal of Experimental Botany 58 (12), 3464–3473.

Hosoi, F., Omasa, K., 2009a. Estimating vertical plant area density profile and growth parameters of a wheat canopy at different growth stages using three-dimensional portable lidar imaging. ISRPS Journal of Photogrammetry and Remote Sensing 64 (2), 151–158.

Hosoi, F., Omasa, K., 2009b. Detecting seasonal change of broad-leaved woody canopy leaf area density profile using 3D portable LIDAR imaging. Functional Plant Biology 36 (11), 998–1005.

Hosoi, F., Omasa, K., 2012. Measurements of vertical plant area density profiles of a rice plant using a portable scanning lidar. Eco-engineering 24 (1), 21–25.

Hosoi, F., Yoshimi, K., Shimizu, Y., Omasa, K., 2005. 3-D measurement of trees using a portable scanning lidar. Phyton – Annales Rei Botanicae 45 (4), 497–500.

Hosoi, F., Nakai, Y., Omasa, K., 2010. Estimation and error analysis of woody canopy leaf area density profiles using 3-D airborne and ground-based scanning lidar remote-sensing techniques. IEEE Transactions on Geoscience and Remote Sensing 48 (5), 2215–2223.

Hosoi, F., Nakabayashi, K., Omasa, K., 2011. 3-D Modeling of tomato canopies using a high-resolution portable scanning lidar for extracting structural information. Sensors 11 (2), 2166–2174. http://dx.doi.org/10.3390/s110202166.

Houldcroft, C.J., Campbell, C.L., Davenport, I.J., Gurney, R.J., Holden, N., 2005. Measurement of canopy geometry characteristics using LiDAR laser altimetry: a feasibility study. IEEE Transactions on Geoscience and Remote Sensing 43 (10), 2270–2282.

Hyyppä, J., Kelle, O., Lehikoinen, M., Inkinen, M., 2001. A segmentation-based method to retrieve stem volume estimates from 3-D tree height models produced by laser scanners. IEEE Transactions on Geoscience and Remote Sensing 39 (5), 969–975.

Imai, K., Shimabe, K., Tanaka, K., 1994. Studies on matter production of edible canna (*Canna edulis* Ker.). Japanese Journal of Crop Science 63 (2), 345–351.

Jones, H.G., 1992. Plants and Microclimate, second ed. Cambridge University Press, Cambridge.

Larcher, W., 2001. Physiological Plant Ecology, fourth ed. Springer, Heidelberg.

Lefsky, M.A., Cohen, W.B., Parker, G.G., Harding, D.J., 2002. Lidar remote sensing for ecosystem studies. Bioscience 52 (1), 19–30.

Lovell, J.L., Jupp, D.L.B., Culvenor, D.S., Coops, N.C., 2003. Using airborne and ground-based ranging lidar to measure canopy structure in Australian forests. Canadian Journal of Remote Sensing 29 (5), 607–622.

Magnussen, S., Boudewyn, P., 1998. Derivations of stand heights from airborne laser scanner data with canopy-based quantile estimators. Canadian Journal of Forest Reserch 28 (7), 1016–1031.

Milroy, S.P., Bange, M.P., Sadras, V.O., 2001. Profiles of leaf nitrogen and light in reproductive canopies of cotton (*Gossypium hirsutum*). Annals of Botany 87 (3), 325–333.

Monsi, M., Saeki, T., 1953. Über den Lichtfaktor in den Pflanzengesellschaften und seine Bedeutung für die Stoffproduktion. Japanese Journal of Botany 14, 22–52.

Monteith, J.L., 1973. Principles of Environmental Physics. Edward Arnold, London.

Morsdorf, F., Kötz, B., Meier, E., Itten, K.I., Allgöwer, B., 2006. Estimation of LAI and fractional cover from small footprint airborne laser scanning data based on gap fraction. Remote Sensing of Environment 104 (1), 50–61.

Næsset, E., Gobakken, T., Holmgren, J., Hyyppä, H., Hyyppä, J., Maltamo, M., Nilsson, M., Olsson, H., Persson, Å., Söderman, U., 2004. Laser scanning of forest resources: the Nordic experience. Scandinavian Journal of Forest Research 19 (6), 482–499.

Norman, J.M., Campbell, G.S., 1989. Canopy structure. In: Pearcy, R.W., Ehleringer, J., Mooney, H.A., Rundel, P.W. (Eds.), Plant Physiological Ecology: Field Methods and Instrumentation. Chapman and Hall, London, pp. 301–325.

Omasa, K., Akiyama, Y., Ishigami, Y., Yoshimi, K., 2000. 3-D remote sensing of woody canopy heights using a scanning helicopter-borne lidar system with high spatial resolution. Journal of Remote Sensing Society of Japan 20 (4), 394–406.

Omasa, K., Urano, Y., Oguma, H., Fujinuma, Y., 2002. Mapping of tree position of Larix leptolepis woods and estimation of diameter at breast height (DBH) and biomass of the trees using range data measured by a portable scanning lidar. Journal of Remote Sensing Society of Japan 22 (5), 550–557.

Omasa, K., Qiu, G.Y., Watanuki, K., Yoshimi, K., Akiyama, Y., 2003. Accurate estimation of forest carbon stocks by 3-D remote sensing of individual trees. Environmental Science & Technology 37 (6), 1198–1201.

Omasa, K., Hosoi, F., Konishi, A., 2007a. 3D lidar imaging for detecting and understanding plant responses and canopy structure. Journal of Experimental Botany 58 (4), 881–898.

Omasa, K., Hosoi, F., Uenishi, T.M., Shimizu, Y., Akiyama, Y., 2007b. Three-dimensional modelling of an urban park and trees by combined airborne and portable on-ground scanning LIDAR remote sensing. Environmental Modeling and Assessment, doi: http://dx.doi.org/10.1007/s10666-007-9115-5.

Parker, G.G., Harding, D.J., Berger, M.L., 2004. A portable LIDAR system for rapid determination of forest canopy structure. Journal of Applied Ecology 41 (4), 755–767.

Pesci, A., Casula, G., Boschi, E., 2012. Laser scanning the Garisenda and Asinelli towers in Bologna (Italy): detailed deformation patterns of two ancient leaning buildings. Journal of Cultural Heritage 12 (2), 117–127.

Pu, S., Vosselman, G., 2009. Knowledge based reconstruction of building models from terrestrial laser scanning data. ISRPS Journal of Photogrammetry and Remote Sensing 64 (6), 575–584.

Radtke, P.J., Bolstad, P.V., 2001. Laser point-quadrat sampling for estimating foliage-height profiles in broad-leaved forests. Canadian Journal of Forest Research 31 (3), 410–418.

Riaño, D., Meier, E., Allgöwer, B., Chuvieco, E., Ustin, S.L., 2003. Modeling airborne laser scanning data for the spatial generation of critical forest parameters in fire behavior modeling. Remote Sensing of Environment 86 (2), 177–186.

Rosell, J.R., Llorens, J., Sanz, R., Arnó, J., Ribes-Dasi, M., Masip, J., Escolà, A., Camp, F., Solanelles, F., Gràcia, F., Gil, E., Val, L., Planas, S., Palacín, J., 2009. Obtaining the three-dimensional structure of tree orchards from remote 2D terrestrial LIDAR scanning. Agricultural and Forest Meteorology 149 (9), 1505–1515.

Strahler, A.H., Jupp, D.L.B., Woodcock, C.E., Schaaf, C.B., Yao, T., Zhao, F., Yang, X., Lovell, J., Culvenor, D., Newnham, G., Ni-Miester, W., Boykin-Morris, W., 2008. Retrieval of forest structural parameters using a ground-based lidar instrument (Echidna®). Canadian Journal of Remote Sensing 34 (2), 426–440.

Takahashi, T., Nakaseko, K., 1993. Seasonal changes in distribution of intercepted photosynthetically active radiation for layer and dry matter production in spring wheat canopy. Japanese Journal of Crop Science 62 (2), 313–318.

Takeda, T., Oguma, H., Yone, Y., Yamagata, Y., Fujinuma, Y., 2005. Comparison of leaf area density measured by laser range finder and stratified clipping method. Phyton – Annales Rei Botanicae 45 (4), 505–510.

Tanaka, T., Park, H., Hattori, S., 2004. Measurement of forest canopy structure by a laser plane range-finding method—improvement of radiative resolution and examples of its application. Agricultural and Forest Meteorology 125 (1–2), 129–142.

Urano, Y., Omasa, K., 2003. Accurate estimation of forest stand parameters in Japanese cedar woods using a portable scanning lidar. In: Proceedings of the IAWPS 2003, Daejeon, Korea, 21–24 April 2003, pp. 403–407.

van der Zande, D., Hoet, W., Jonckheere, I., van Aardt, J., Coppin, P., 2006. Influence of measurement set-up of ground-based LiDAR for derivation of tree structure. Agricultural and Forest Meteorology 141 (2–4), 147–160.

Webster, T.L., Murphy, J.B., Gosse, J.C., Spooner, I., 2006. The application of lidar-derived digital elevation model analysis to geological mapping: an example from the Fundy Basin, Nova Scotia, Canada. Canadian Journal of Remote Sensing 32 (2), 173–193.

Weiss, M., Baret, F., Smith, G.J., Jonckheere, I., Coppin, P., 2004. Review of methods for in situ leaf area index (LAI) determination. Part II. Estimation of LAI, errors and sampling. Agricultural and Forest Meteorology 121 (1–2), 37–53.

Welles, J.M., Cohen, S., 1996. Canopy structure measurement by gap fraction analysis using commercial instrumentation. Journal of Experimental Botany 47 (302), 1335–1342.

Welles, J.M., Norman, J.M., 1991. Instrument for indirect measurement of canopy architecture. Agronomy Journal 83 (5), 818–825.

Yunusa, I.A.M., Siddique, K.H.M., Belford, R.K., Karimi, M.M., 1993. Effect of canopy structure on efficiency of radiation interception and use in spring wheat cultivars during the pre-anthesis period in a Mediterranean-type environment. Field Crops Research 35 (2), 113–122.